



Mitigating autogenous shrinkage of cement paste with novel shrinkage-reducing polycarboxylate superplasticizer

Jian Zhang · YueFeng Ma · Haixin Zhao · Huaqiang Sun · Jiaping Liu

Received: 7 April 2022 / Accepted: 18 October 2022 / Published online: 28 October 2022
© The Author(s) 2022

Abstract This study aims to disclose the working mechanisms of a novel shrinkage-reducing polycarboxylate superplasticizer (SR-PCA) in mitigating autogenous shrinkage of cement paste. The properties of pore solutions (-including the surface tension and contact angle), ions concentration in pore solutions, internal relative humidity (RH), dynamic elastic modulus, pore structure characteristic and autogenous shrinkage are thoroughly investigated. The results indicate that SR-PCA substantially reduces the autogenous shrinkage of cement paste. From the perspective of pore solution properties, SR-PCA increases the hydrophobicity of the pore solution and reduces the surface tension, thus lowering the internal RH depression, capillary stress development and autogenous

shrinkage of the cement paste. Also, SR-PCA reduces the volume fraction of mesopore (pore size less than 50 nm) where the capillary stress is exerted, thereby lowering autogenous shrinkage. Moreover, the presence of SR-PCA increases the expansion stress mainly induced by portlandite, reduces the capillary stress and enhances the dynamic elastic modulus of cement pastes, contributing to controlling autogenous shrinkage.

Keywords Autogenous shrinkage · Pore solution properties · Surface tension · Contact angle · Shrinkage-reducing polycarboxylate superplasticizer (SR-PCA)

J. Zhang
Key Laboratory for Resilient Infrastructures of Coastal Cities (MOE), College of Civil and Transportation Engineering, Shenzhen University, Shenzhen 518060, China

J. Zhang · J. Liu (✉)
School of Materials Science and Engineering, Southeast University, Nanjing 211189, China
e-mail: liujiaping@cnjsjk.cn

Y. Ma · H. Zhao
College of Materials Science and Engineering, Chongqing University, Chongqing 400045, China

H. Sun
School of Advanced Manufacturing, Fuzhou University, Quanzhou 362200, China

1 Introduction

Currently, polycarboxylate superplasticizers (PCs) are crucial ingredients of high-performance concrete and are widely used in various modern concrete construction. Although the primary role of PCs is the improvement of the workability and mechanical properties of concretes [1–4], they may be detrimental to the volume stability of cementitious materials [1, 5–8]. One effective solution to restrain shrinkage crack is incorporating shrinkage-reducing admixtures (SRAs), which can control the shrinkage by lowering the surface tension of the pore solution [9–11]. However, some adverse side effects have also been



observed. More specifically, SRAs delay the cement hydration and strength development of cementitious materials [12–14]. It has also been found that SRAs play a negative side role in the frost resistance of concrete due to entrained air loss [15–17]. Additionally, the effectiveness of SRAs may be overshadowed owing to poor compatibility with PCs [18]. Hence, a more appropriate method should be sought to address the problems above.

Shrinkage-reducing polycarboxylate superplasticizers (SR-PCAs) have been designed by grafting the shrinkage-reducing groups into the main chain with carboxylic groups. Typically, SR-PCAs are prepared by copolymerizing the unsaturated acid and shrinkage-reducing function monomers, which can thoroughly solve the incompatibility between PCs and SRAs. In the last few years, various investigations have been carried out to study the performance of SR-PCAs in cementitious materials. Zuo et al. [19] reported that a polyether-type SRA had a remarkable retardation effect on cement hydration and maintained a high internal RH in cement paste, resulting in a significant decrease in capillary stress and autogenous shrinkage. However, the water-reducing capability of polyether-type SRA is not good enough. In fact, it is still a shrinkage-reducing admixture but not a shrinkage-reducing polycarboxylate superplasticizer. Yang et al. [20] studied the impact of a shrinkage-reducing polycarboxylate admixture SRPCA on the cracking reduction mechanism by a temperature stress testing machine. This shrinkage-reducing polycarboxylate admixture needs to co-add with polycarboxylate superplasticizer to achieve target workability, implying its poor water reduction function. Ran et al. [8] designed a multi-functional superplasticizer JM-PCA with a shrinkage-reducing function. However, its shrinkage-reducing capability needs to be further improved. Mao et al. [21, 22] claimed that novel shrinkage-reducing polycarboxylate SRPC delayed cement hydration. They also found that the adsorption capability of SRPC was inferior to that of the conventional polycarboxylate superplasticizer, while the shrinkage-reducing capability was far superior to that of the conventional polycarboxylate superplasticizer. Besides, the shrinkage-reducing capability of SRPC could arise from reducing surface tension and regulating the pore size distribution. To sum up, the shrinkage-reducing or water-reducing capability of the abovementioned chemical admixtures is not good

enough to use alone in cement-based materials. The development of SR-PCAs with excellent shrinkage-reducing and water-reducing performance is still a research hotspot. Moreover, the limited studies on the shrinkage behavior of SR-PCAs lack a comprehensive and systematic understanding of the shrinkage-reducing mechanisms.

Like SRAs, capillary tension theory is generally used to interpret the shrinkage-reducing mechanism of SR-PCAs, in which substantial insights into the surface tension of the pore solution have been gained [19, 23, 24]. Nevertheless, another important pore solution property that also influences volume deformation is the contact angle between the pore wall and pore solution. The modification of the contact angle by adding polymers can change the capillary stress in the porous medium, thereby affecting the shrinkage deformation. Bentz et al. [14] reported that the contact angle was delined from 28° to 7° by incorporating SRA. Wang et al. [25] found that the increase of the contact angle was one of the reasons for SRA to mitigate the shrinkage. This controversy about the change of contact angle with the incorporation of polymers may be remarkably influenced by the structure and properties of polymers.

In order to disclose the autogenous shrinkage mitigation mechanisms of SR-PCAs comprehensively, this work was conducted in the following three parts. Firstly, the surface tension and the contact angle of the pore solution were characterized. Secondly, pore structure characteristic, mainly considering the volume fraction of capillary pores less than 50 nm, was analyzed to interpret the impact of SR-PCAs on the pores where the capillary pressure is mainly exerted. Finally, the development of expensive stress and capillary pressure was calculated by analyzing the ions concentrations in the pore solution and relative humidity (RH) development, respectively. Based on the elastic modulus results and the modified Biot-Bishop model, the simulated autogenous shrinkage of cement paste with SR-PCA was obtained.

2 Materials and methods

2.1 Materials and mix proportion

The main mineral phase composition of P-I Portland cement used in the present work was 41.12 wt% C₃S,



Table 1 Mix proportions of the cement paste mixtures

Mixture ID	w/c	PCA (wt%)	SR-PCA(wt%)
C-REF	0.29		
C-PCA	0.29	0.08	
C-SR-PCA	0.29		0.40

31.86 wt% C₂S, 2.15 wt% C₃A, 10.56 wt% C₄AF. The physical properties and chemical structure of the novel SR-PCA used here can be found in [26]. For comparison, a commercial polycarboxylate superplasticizer PCA was also employed. The difference between the two chemical admixtures was that SR-PCA had a stronger hydrophobicity than PCA, as reported in reference [26].

Three mixtures were investigated in this work (see Table 1). C-REF mixture, C-PCA mixture and C-SR-PCA mixture denote the reference cement paste, the cement pastes with PCA and SR-PCA, respectively. Here, the fluidity of C-PCA mixture was 240 ± 10 mm, which was in accord with the C-SR-PCA mixture.

2.2 Pore solution properties

According to the reference [25], the supernatant of the cement slurry could be used to simulate the actual pore solution in the cementitious materials. Firstly, the cement was well mixed with water with a ratio of 1: 2 by weight, and then it was settled for 30 min. When the solid and solution were completely separated, the upper supernatant was filtered and collected to test the solution properties as follows.

2.2.1 Surface tension

The pore solution (~ 40 mL) was collected and measured using a surface tension analyzer K100 (KRUSS, Germany) at 20 °C.

2.2.2 Contact angle

The contact angle measurement was conducted on a contact angle tester DSA255 (KRUSS, Germany) by the sessile drop method [25]. Firstly, a 1 ml syringe was used to control the liquid droplet. Once the droplet was full, it was attracted to a piece of sample cured for

3 days with a diameter of 8 cm. After that, an image was taken at 60 s, and then the contact angle of the droplet was determined.

2.3 Pore structure characteristics

The pore structure characteristics of samples were carried out on AutoPore V 9620 mercury intrusion porosimetry (Micromeritics, USA). The samples were cured for 3 days and 28 days, then cut into 4 mm \sim 6 mm cubes, put into isopropanol for 3 days to stop hydration and dried at 45 °C for 7 days before measurements. The testing pressure ranged from 0 to 414 MPa.

2.4 Ions concentration analysis

Pore solution was obtained by high-pressure steel die at the determined ages. To avoid carbonation and potential reactions, the pore solution was collected and sealed in a plastic bottle immediately after extraction, then was stored under 5 °C before measurement. The K⁺, Na⁺ and Ca²⁺ ions concentrations were determined by Inductively Coupled Plasma Optical Emission Spectrometer (ICP-OES) (SPECTRO Analytical Instruments, Germany). The TOSOH IC-2010 ion chromatography (TOSOH, Japan) and PHS-3E pH meter (REX, China) were used for SO₄²⁻ and OH⁻ analysis, respectively.

2.5 Relative humidity (RH)

The evolution of the RH in the mixtures was obtained by a Humidity Recorder. Before measurements, relative humidity sensors were calibrated using saturated NaCl, KCl and K₂SO₄ solutions. When the mixture reached the final setting time, the relative humidity sensor was embedded into a 6 cm depth of the hole (prefabricated by a solid PVC rod) and sealed with aluminum foil. Besides, the ambient temperature was constant at 20 °C during the RH measurement. The RH value was recorded at 5 min intervals.

2.6 Dynamic elastic modulus

According to the reference [27], the dynamic elastic modulus E could be calculated with the ultrasonic wave speed using Eq. (1).

$$E = \frac{(1 + \nu)(1 - 2\nu)}{(1 - \nu)} \rho C_L^2 \quad (1)$$

where ν is the Poisson's ratio, here, it is assumed as 0.22. ρ is the density of mixture. C_L is the ultrasonic wave speed, which is determined by a NELD-DTV non-metal ultrasonic tester (NELD, China).

2.7 Autogenous shrinkage

Autogenous shrinkage was determined by corrugated polyethylene tubes (Φ 30 mm \times 400 mm) at 20 °C, as reported in the reference [28]. The SBT-AS200 tester (SBT, China) was applied to record the autogenous shrinkage deformation. The data was collected every 5 min. According to the reference [29], the final setting time was set as the starting point for analyzing the autogenous deformation. In this work, the final setting time of C-REF, C-PCA and C-SR-PCA were 4.3 h, 4.3 h and 7.6 h, respectively.

3 Results

3.1 Pore solution properties

3.1.1 Surface tension

Figure 1 presents the surface tension of the pore solution for three mixtures. Note that the surface tension of the pore solution is 69 mN/m. With the presence of PCA and SR-PCA, the surface tension of the pore solution is reduced to 65 mN/m and 32 mN/m, corresponding to the polymer concentration is 0.04% and 0.2%, respectively. This indicates that SR-PCA reduces the surface tension significantly. In our previous study [26], 0.35 M KOH and 0.05 M NaOH were mixed to simulate the pore fluid in the cementitious system [15]. The surface tension of these pore solutions with SR-PCA is higher than 50 mN/m at the lowest. However, in this work, the supernatant of the cement slurry was used to simulate the pore solution in cement paste. Therefore, the different measured value of surface tension is mainly attributed to the various simulation method of pore solution. Although the measured value of surface tension in the two ways differs, both indicate that SR-PCA has a stronger ability to reduce surface tension than PCA. This is partly attributed to SR-PCA delaying the cement

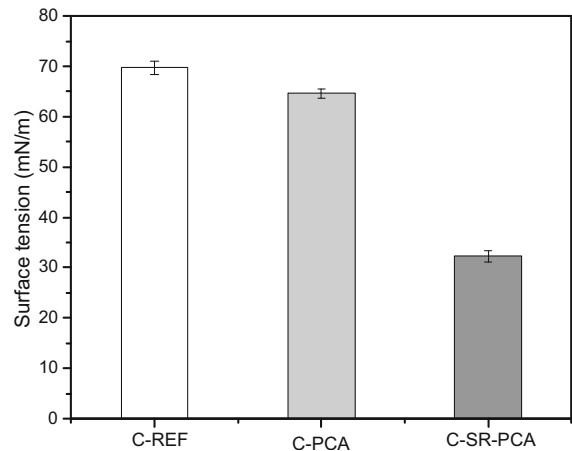


Fig. 1 Surface tension of pore solution for various cement pastes

hydration reaction and the dissolution of ions, reducing the repulsive force from the air-solution interface and increasing the amount of SR-PCA at the surface [30]. Another reason may be owing to the higher hydrophobicity of SR-PCA [26], which can arrange more SR-PCA molecules at the interface of air-water, in turn decreasing the surface tension [19, 31]. It has also been reported that decreasing the surface tension of the pore solution can cause capillary stress reduction, thus mitigating the shrinkage [32, 33].

3.1.2 Contact angle

The contact angle of pore solution for various cement pastes is shown in Fig. 2. PCA and SR-PCA increase the contact angle from 28.1° to 32.7° and 75.3°, respectively. As expected, the contact angle in the C-SR-PCA mixture is increased significantly due to the higher hydrophobicity of SR-PCA [34, 35]. The result demonstrates that SR-PCA substantially impacts the wetting resistance of cement pastes, and it renders the pore solution of pastes more hydrophobic.

3.2 Ionic concentrations

Figure 3 shows the ions concentration in the pore solution of various cement pastes. Notably, all ions in the pore solution of C-PCA have a similar concentration to that in the plain mixture. Compared with C-SR-PCA, the C-REF mixture and C-PCA mixture show

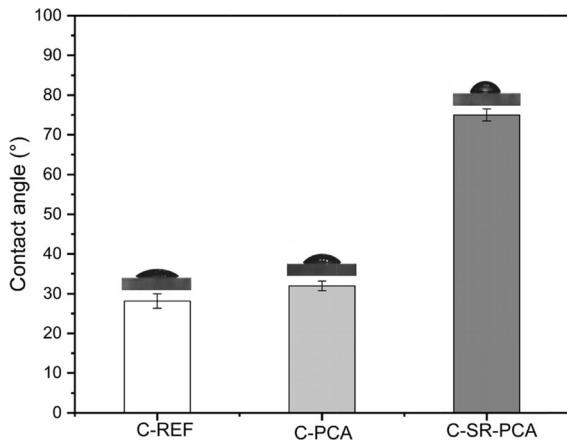


Fig. 2 Contact angle of pore solution for various cement pastes

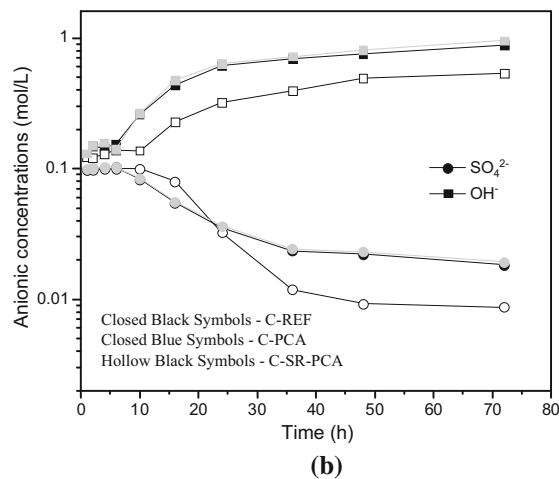
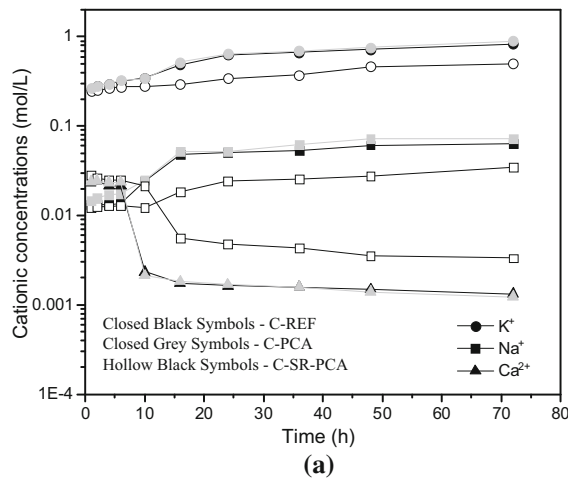


Fig. 3 Evolution of ions concentration in the pore solution: **a** cations and **b** anions

higher alkali ions (K^+ and Na^+) concentrations. In contrast, C-SR-PCA exhibits a higher Ca^{2+} concentration than them, which is consistent with the findings in references [15, 36, 37].

The variation of anion (SO_4^{2-} and OH^-) concentrations is presented in Fig. 3b. Initially, the C-REF mixture exhibits a little higher SO_4^{2-} concentration compared to the C-SR-PCA mixture. However, the difference is nearly constant until the solid gypsum is completely consumed, at around 6 and 10 h for C-REF and C-SR-PCA mixture, respectively [38]. After that, the SO_4^{2-} concentrations in solutions reduce monotonically and dramatically. As for OH^- concentrations, there is a similar tendency with the evolution of SO_4^{2-} concentrations in all samples before the complete consumption of solid gypsum. After that, OH^- concentration in all cases increases sharply. Moreover, the OH^- concentration in the C-SR-PCA mixture is consistently lower than that in the C-REF mixture and C-PCA mixture. The lower OH^- concentration in the C-SR-PCA mixture is expected to delay the C_3A dissolution and retard C_3S hydration, which agrees with the findings in references [15, 36].

3.3 Dynamic elastic modulus

The dynamic elastic modulus of various cement pastes and the corresponding regression equations parameters are presented in Fig. 4 and Table 2, respectively. The dynamic elastic modulus of all mixtures displays an increasing trend during the test. However, the development rate of dynamic elastic modulus in all samples gradually drops with time. Besides, PCA has negligible influence on the dynamic elastic modulus before 72 h, while SR-PCA reduces the dynamic elastic modulus remarkably. Eventually, SR-PCA and PCA can slightly improve the elastic modulus of the mixtures at 7d. In addition, considering the ageing effect, the following prediction equation for dynamic elastic modulus is proposed.

$$E(t) = a * \exp * (b/(t + c)) \quad (2)$$

where $E(t)$ is the dynamic elastic modulus after curing ages t h; a , b and c are the constants, which can be obtained by regression analysis (see Table 2).

From Table 2, the correlation coefficients R^2 of the regression equations are greater than 0.98, which indicates a good correlation between the dynamic elastic modulus and regression equations. Hence,

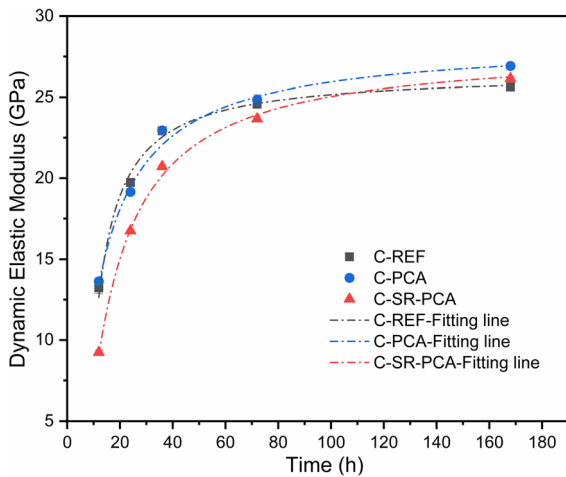


Fig. 4 Evolution of dynamic elastic modulus for various cement pastes

Table 2 Parameters and correlation coefficients from regression analysis based on Eq. (2)

Mix	a	b	c	Coefficient of determination
C-REF	26.52	- 4.99	- 5.26	$R^2 = 0.982$
C-PCA	28.45	- 9.28	- 0.43	$R^2 = 0.996$
C-SR-PCA	28.09	- 11.26	- 2.02	$R^2 = 0.997$

these regression equations can be used to calculate the autogenous shrinkage, as shown in Sect. 4.4.

3.4 RH

The evolution of RH in C-REF, C-PCA and C-SR-PCA mixtures is presented in Fig. 5. Initially, RH of C-REF, C-PCA and C-SR-PCA is 97.7%, 98.5% and 99.0%, respectively. Then the RH declines quickly in the first 7 days and decreases gradually with the elapse of time. The decline of RH in cement paste is retarded significantly with the addition of SR-PCA, while it is slightly influenced by PCA. On the one hand, it can be ascribed to their effect on cement hydration. As shown in a previous study [26], SR-PCA significantly retarded cement hydration, whereas PCA slightly impacts cement hydration. On the other hand, it is commonly reported that reducing the surface tension of the pore solution is vital to maintaining the RH and controlling the autogenous shrinkage [19, 33]. According to Fig. 1 and Kelvin equation (Eq. (2)),

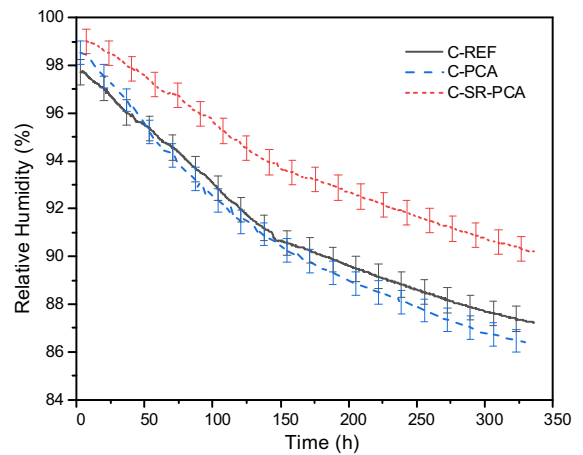


Fig. 5 Evolution of RH in various cement pastes

the surface tension of pore solution is decreased sharply by adding SR-PCA, corresponding to a higher RH in C-SR-PCA mixture. This again confirms the effectiveness of SR-PCA in maintaining a relatively high RH.

3.5 Autogenous shrinkage

Figure 6 presents the autogenous shrinkage of various cement pastes. Notably, SR-PCA mitigates the autogenous shrinkage remarkably, whereas PCA significantly increases the autogenous shrinkage. More specifically, the autogenous shrinkage of cement paste at 7d is reduced by 12.2% and increased by 19.90% with the addition of SR-PCA and PCA, respectively.

4 Discussion

4.1 Proposal of a mitigating shrinkage mechanism based on pore solution properties

Generally, the menisci can form due to moisture loss during the cement hydration or drying process. Then the capillary pressure is elevated, thereby inducing the shrinkage of cementitious materials [39, 40]. According to Eqs. (3) and (4), capillary pressure can be obtained.

$$\sigma = -\frac{2\gamma \cos \theta}{r} \tag{3}$$

$$\ln RH = -\frac{2\gamma V_w \cos \theta}{rRT} \tag{4}$$



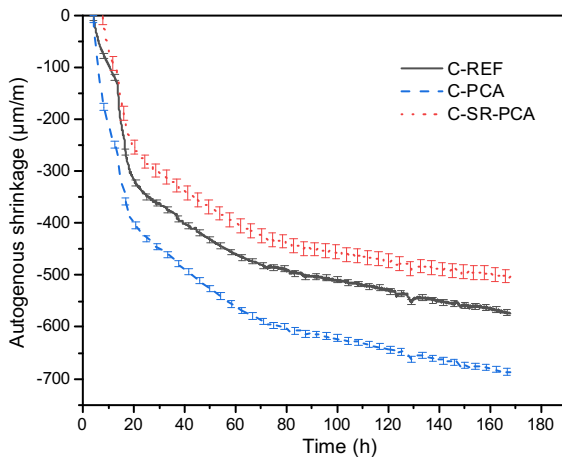


Fig. 6 Autogenous shrinkage of various cement pastes. (To improve readability, the standard deviation bars for mixtures are only shown for every fiftieth data point.)

where σ represents the capillary pressure (Pa), γ represents the surface tension of pore solution (N/m), θ denotes the contact angle ($^\circ$), r denotes the menisci curvature radius (m), RH denotes the internal relative humidity (%). Here, V_w , R and T are assumed to be $1.802 \times 10^{-5} \text{ m}^3/\text{mol}$, $8.314 \text{ J}/(\text{mol}\cdot\text{K})$ and 293.15 K , respectively.

Considering the shrinkage mechanism in the cement-based materials using Eqs. (3) and (4), the pore solution is commonly assumed to be water. Namely, the contact angle θ is always regarded as 0 [33, 41, 42], and the surface tension is usually taken as 72.0 N/m . In this case, with regard to the shrinkage-reducing mechanism, the property of the pore solution has been overlooked for a long time. A systematic study is conducted to investigate the effect of SR-PCA on RH evolution and capillary pressure development. The results in Fig. 7 show the impact of contact angle and surface tension on the RH and capillary pressure is mainly exerted on the pores with a size less than 50 nm , which is in line with other studies [34, 43]. In this range of pores, the RH increases and capillary pressure decreases as the hydrophobicity of pore solution increases and the surface tension declines. That is, the presence of SR-PCA maintains the RH at a higher level and reduces the capillary pressure, which is also confirmed by the evolution of internal RH (see Fig. 5) From the perspective of pore solution properties, SR-PCA can control the autogenous by increasing the hydrophobicity and decreasing the surface tension of the pore solution.

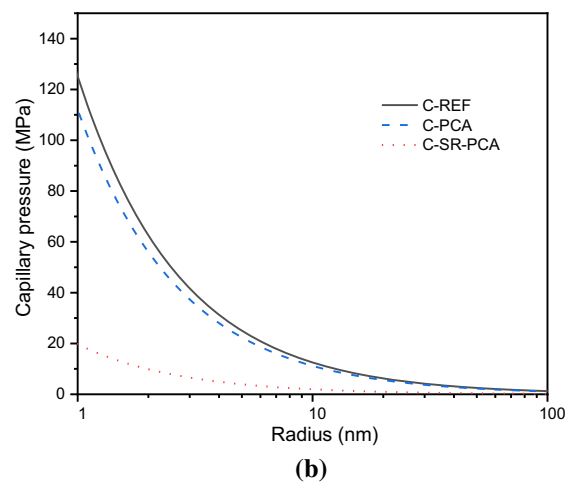
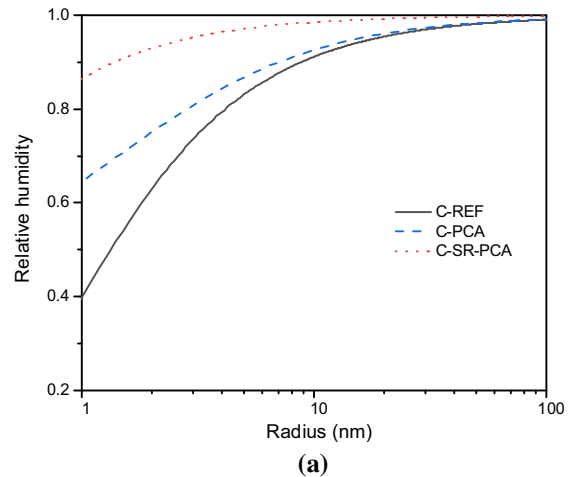


Fig. 7 Evolution of **a** RH and **b** capillary pressure for the cement pastes with different contact angles and surface tension

4.2 Effect of SR-PCA on the pore structure

The pore size distribution of different mixtures is shown in Fig. 8. From a previous study [26], the total porosity of the C-REF, C-PCA and C-SR-PCA is 26.7%, 24.8% and 27.4% at 1 day, 25.9%, 22.6% and 25.4% at 3 days, 21.8%, 20.9% and 20.5% at 28 days, respectively. The results show that PCA can refine pore structure during the curing time. However, SR-PCA coarsens the pore structure before 3 days and refines it after 3 days, resulting from its retardation effect on the cement hydration. According to the classification principle in the references [44, 45], the mesopore volume fraction (pore size less than 50 nm) of C-REF, C-PCA and C-SR-PCA is 56.8%, 57.2% and 46.9% at 1 day, 60.2%, 58.3% and 50.6% at

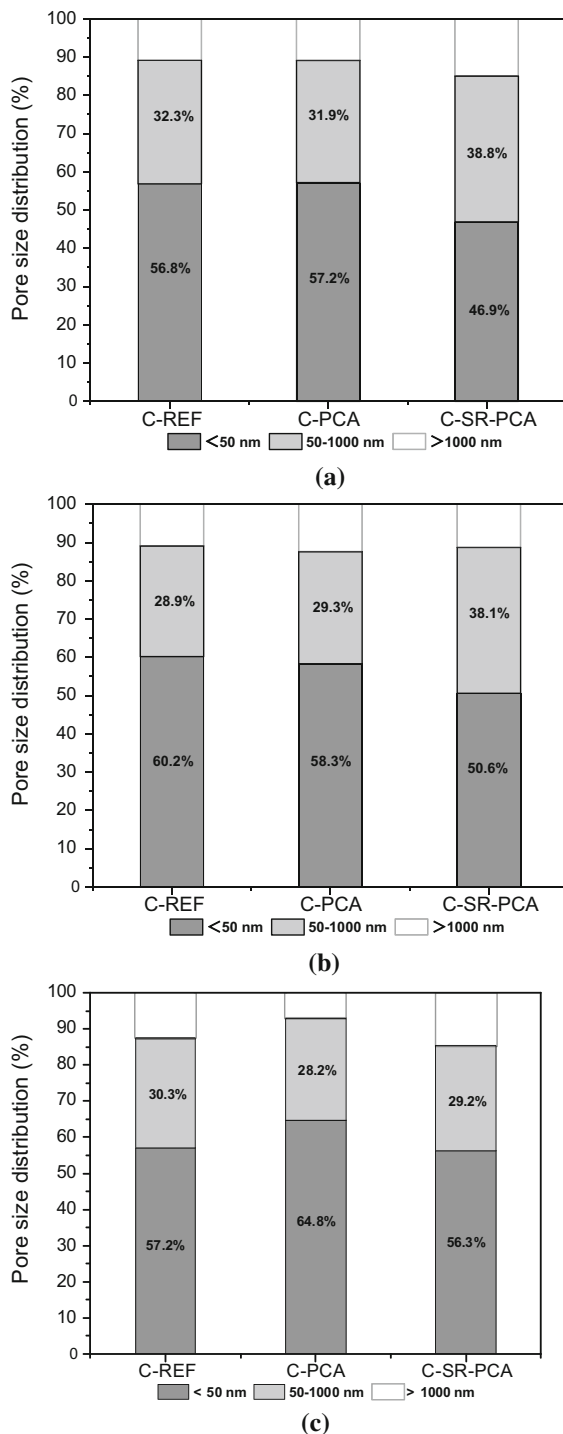


Fig. 8 Pore size distribution for cement pastes at **a** 1d, **b** 3d and **c** 28d

3 days, 57.2%, 64.8% and 56.3% at 28 days, respectively. Based on the results from Sect. 4.1 and references [44–47], capillary stress is generally exerted on the pores with a size of less than 50 nm. That is, the mesopore volume fraction is another critical factor in controlling the shrinkage of cementitious materials. With the presence of SR-PCA, the 1d, 3d and 28d mesopore volume fractions of cement paste are reduced by 9.9%, 9.6% and 0.9%, respectively. This indicates that SR-PCA can lower autogenous shrinkage by reducing the mesopore volume fraction.

4.3 Effect of SR-PCA on the development of expansion stress

4.3.1 Effective phase saturation index (SI)

The saturation level of various phases in cement paste is commonly described by SI, which can be obtained from Eq. (5). The positive value and negative value of SI indicate oversaturation and undersaturation, corresponding to a solid phase and dissolution, respectively. When SI equals zero, it implies the dynamic equilibrium between dissolution and precipitation.

$$SI = \frac{1}{N} \cdot \log \left(\frac{IAP}{K_{SP}} \right) \quad (5)$$

where IAP and K_{sp} represent the ion-activity product of various phases and theoretical solubility product, respectively. N represents the number of ionic species participating in dissolution. IAP can be calculated by the thermodynamic software GEMS [48], K_{sp} and N are obtained from reference [36].

Figure 9 illustrates the SI for various phases in C-REF and C-PCA and C-SR-PCA mixtures. In all cases, ettringite and portlandite show positive SI values, signifying the oversaturation of ettringite and portlandite throughout the observed 72 h. However, the SI curves of gypsum and monosulfate decrease monotonically and show a negative value at last. Besides, the depletion of gypsum for the plain mixture and C-SR-PCA mixture is at 6 h and 10 h, respectively. This delay of gypsum depletion confirms the retardation effect of SR-PCA on cement hydration,

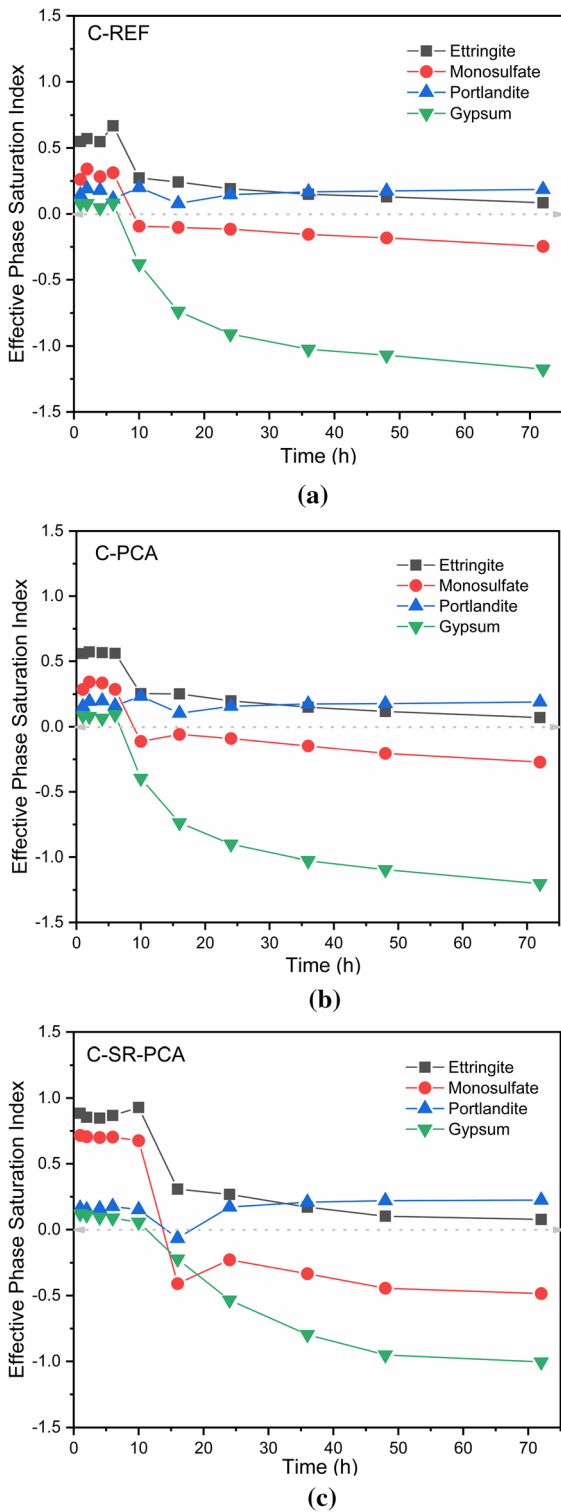


Fig. 9 Development of SI for various phases obtained from ions concentrations in the pore solutions: **a** C-REF, **b** C-PCA and **c** C-SR-PCA

which agrees with the ionic concentration results in Sect. 3.2. It should also be noted that SR-PCA leads to higher SI for ettringite and portlandite throughout the test. This higher SI is closely associated with reducing alkali and SO_4^{2-} concentrations and increasing Ca^{2+} concentrations in pore solution [15, 49]. Further, the higher oversaturations for ettringite and portlandite in the C-SR-PCA mixture are expected to induce a remarkable crystallization pressure and expansion deformation at the early ages of cement hardening.

4.3.2 Crystallization pressure

When a crystalline phase is oversaturated in solution, it will precipitate and grow under crystallization pressure, which can be estimated by Eq. (6).

$$\sigma_c = \frac{RT}{V'_m} \cdot \ln\left(\frac{IAP}{K_{SP}}\right) \tag{6}$$

where σ_c denotes crystallization pressure (MPa), V'_m denotes the molar volume of various phases. Here, the molar volume of portlandite and ettringite is $33 \text{ cm}^3/\text{g}$ and $707 \text{ cm}^3/\text{g}$, respectively [36].

Figure 10 depicts the crystallization pressure exerted by crystal phases. Note that the crystallization pressure curves exhibit a similar tendency to SI curves. Namely, the crystallization pressure of ettringite consistently declines, while that of portlandite decreases at first and then increases with time [50, 51]. It can be seen from Fig. 10a that the crystallization pressures of portlandite in the C-REF, C-PCA and C-SR-PCA mixtures are around 98 MPa, 96 MPa and 115 MPa, respectively. Nevertheless, the calculated crystallization pressures of ettringite in the three mixtures are around 8 MPa. Therefore, it can be deduced that the portlandite mainly dominate the crystallization pressures in three mixtures [36].

4.3.3 Expansive stress

When calculating the expansive stress developed in the pores of the cement matrix, the crystalline stresses of the crystalline phases and its volume fraction occupying the cement paste system should be considered. The expansive stress can be obtained by Eq. (7) [52, 53]:

$$\sigma_{ec} = \sigma_c \cdot S_c = \sigma_c \cdot \left(\frac{R\varphi_c}{\varphi_t}\right) \tag{7}$$



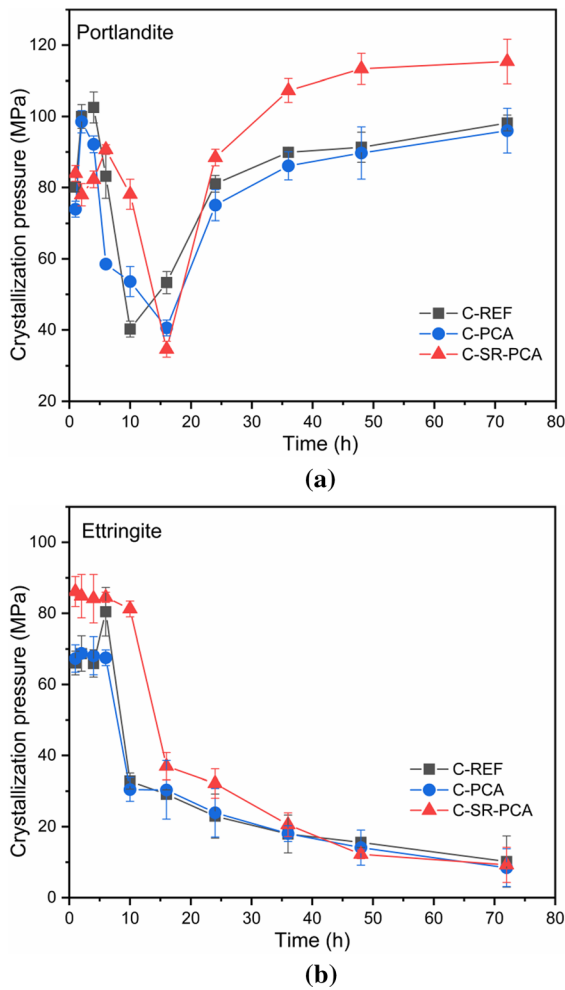


Fig. 10 Evolution of crystallization pressure exerted by the crystal phases: **a** portlandite and **b** ettringite

where σ_{ec} represents the expansive stress (MPa), S_c represents the fraction of the pore occupied by the crystalline phase, σ_c is crystalline pressure obtained from Eq. (6), φ_c represents the fraction of the crystalline phases in the cement paste matrix (%), which can be obtained according to the GEMS. R is defined as the fraction of the crystalline phase growing in the pores and causing expansion. This parameter is arbitrary and difficult to measure. Herein, R is assumed to be 100%, indicating all the crystalline phases growing in the pores can generate the expansion stress, as coincided with the reference [19]. φ_t denotes the total porosity, which can be obtained according to the Powers model and the hydration degree results from the reference [26].

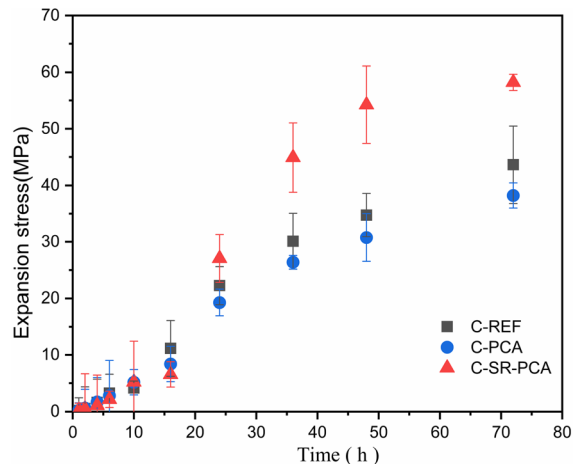


Fig. 11 Evolution of expansion stress developed in the microstructure of various cement pastes

Figure 11 presents the expansion stress developed in the microstructure of the plain mixture, C-PCA and C-SR-PCA mixtures. It should be noted that the C-SR-PCA exhibits similar expansion stress to the plain mixture and C-PCA mixture before 10 h. Then the expansion stress of all mixtures shows a monotonous increase with time, corresponding to the crystalline stress of portlandite increasing. This again indicates that expansion stress in three mixtures is mainly caused by the portlandite phase, which is consistent with the results in the references [19, 36]. Finally, SR-PCA increases expansion stress in the cement paste at 72 h by 33.4%, while PCA reduces expansion stress by 12.4% with respect to the plain mixture. Consequently, the increase of expansion stress in the C-SR-PCA mixture contributes to SR-PCA mitigating autogenous shrinkage of cement paste.

4.4 Effect of SR-PCA on shrinkage stress and autogenous shrinkage simulation

Autogenous shrinkage is often defined as the apparent volume change due to capillary pressure, which is induced by internal RH depression. Hence, it is common to simulate autogenous shrinkage by measuring the variation of internal RH. However, the measured RH (Fig. 5) is generally influenced by the ionic strength of the pore solution, the relationship between them is described by Eq. (8).

$$RH_m = RH_s \cdot RH_k \tag{8}$$

where RH_m refers to the measured internal RH (%),



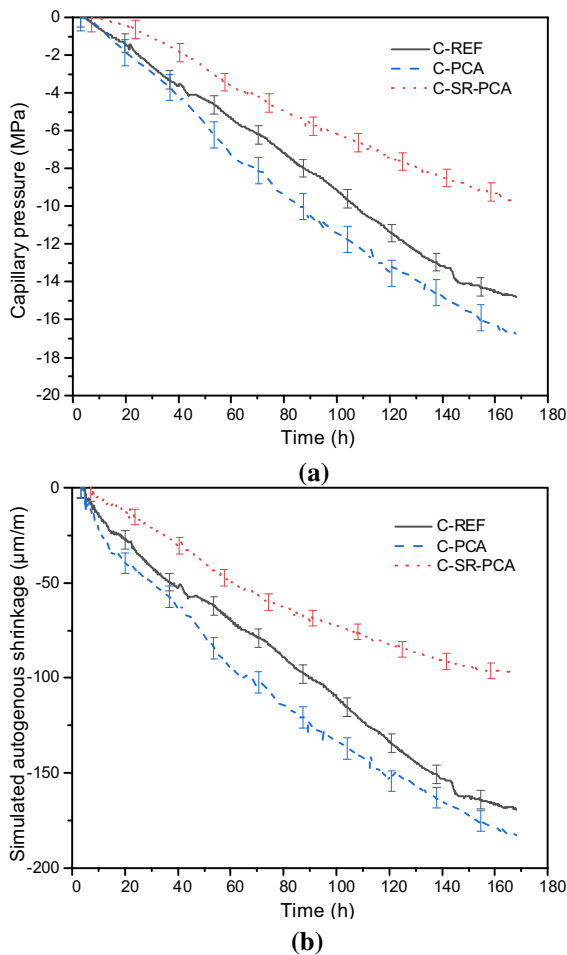


Fig. 12 Calculated **a** capillary pressure and **b** autogenous shrinkage of various cement pastes

RH_s represents the RH depression due to ions in the pore solution. From Sect. 3.4, the RH_s is 97.7%, 98.5% and 99.0% for the plain mixture, C-PCA mixture and C-SR-PCA mixture, respectively. RH_k is the RH depression due to the consumption of pore solution. Further, the shrinkage stress induced by self-desiccation (σ_{RH}) can be described based on Eqs. (3) and (8), and shown in Eq. (9) and Fig. 12a.

$$\sigma_{RH} = -\frac{\ln(RH_k)RT}{V_w} \quad (9)$$

In closing, the deformation of cement pastes ε_{AD} can be simulated using a modified Biot-Bishop model, as shown in Eq. (10) [54].

$$\varepsilon_{AD} = \frac{S_w \sigma_{RH} (1/K - 1/K_s)}{3} \quad (10)$$

where S_w denotes saturation fraction, which can be calculated using the Powers model [42]. K represents the bulk modulus of the cement matrix (GPa), which can be described as $K = E/3(1 - 2\nu)$. Here, ν is assumed as 0.22 [36, 55], E refers to the dynamic elastic modulus displayed in Sect. 3.3. K_s represents the bulk modulus of the solid skeleton in the cement matrix (assuming equal to 44 GPa) [56].

According to Eq. (10) and the results above, the simulated autogenous shrinkage of the C-REF, C-PCA and C-SR-PCA mixtures is depicted in Fig. 12b. The simulated autogenous shrinkage of the plain mixture, C-PCA mixture and C-SR-PCA mixture at 7d are around 169, 182 and 96 microstrains, respectively, which are 3.4, 3.8 and 5.2 times lower than the measured value (see Fig. 6), respectively. Zuo et al. [19] and Sant et al. [36] found that the calculated shrinkage values of pastes containing a shrinkage-reducing admixture are around 6 times lower than the measured values, which is a similar discrepancy value to the result here.

The discrepancies between the measured and simulated autogenous shrinkage may arise from underestimating the shrinkage stress developed in the pore space of the cement matrix. This underestimation may be associated with the uncertainties in the measurement of RH at very early ages and the assessment of the global state of the system by the local measurement. Further, this autogenous shrinkage model assumes that cement pastes are elastic materials, neglecting the significant viscoelastic effect (i.e., creep). Also, there may be other mechanisms that drive autogenous shrinkage. As such, further research should be conducted to find out the potential driving force of autogenous shrinkage, in turn improving modelling accuracy. Although the magnitude of calculated deformation does not capture well the measured results, it is also worthwhile to depict the effectiveness of PCA and SR-PCA on shrinkage reduction.

5 Conclusions

In this work, a comparative study is conducted between a novel shrinkage-reducing polycarboxylate superplasticizer SR-PCA and a traditional

polycarboxylate superplasticizer PCA to investigate their effect on the autogenous shrinkage of cement pastes. Additionally, the underlying mitigation shrinkage mechanisms of SR-PCA are disclosed. The conclusions are drawn as follows:

1. The autogenous shrinkage of cement paste is reduced by 12.2% with the presence of SR-PCA, whereas it is increased by 19.9% with the incorporation of PCA.
2. From the perspective of pore solution properties, SR-PCA increases the hydrophobicity of the pore solution and reduces the surface tension, leading to maintaining a higher internal RH, lowering the capillary pressure and autogenous shrinkage of cement paste.
3. The pore solution properties results indicate the internal RH evolution and capillary pressure development are mainly exerted on the mesopores (pore size less than 50 nm). SR-PCA can reduce the mesopore volume fraction, thereby lowering autogenous shrinkage.
4. Compared with the plain mixture, the 72 h expansion stress of mixture with SR-PCA is increased by 33.4%, while that of the mixture with PCA is decreased by 12.4%. Furthermore, the effectiveness of SR-PCA on autogenous shrinkage can also be interpreted by the synergistic effects of improving expansion stress, decreasing the shrinkage stress and increasing the dynamic elastic modulus.

Acknowledgements The authors would like to acknowledge financial assistance from the Graduate Research and Innovation Foundation of Chongqing, China (CYB22001). The authors also would like to thank Ning Wang from Shiyanjia Lab (www.shiyanjia.com) for the ICP-OES measurement.

Declarations

Conflict of interest The authors declare that they have no conflict of interest.

References

1. Ma BG, Wang XG, Li XG, Yang L (2007) Influence of superplasticizers on strength and shrinkage cracking of cement mortar under drying conditions. *J Wuhan Univ Technol* 22:358–361. <https://doi.org/10.1007/s11595-005-2358-6>
2. Yamada K, Ogawa S, Hanehara S (2001) Controlling of the adsorption and dispersing force of polycarboxylate-type superplasticizer by sulfate ion concentration in aqueous phase. *Cem Concr Res* 31:375–383. [https://doi.org/10.1016/S0008-8846\(00\)00503-2](https://doi.org/10.1016/S0008-8846(00)00503-2)
3. Sakai E, Ishida A, Ohta A (2006) New trends in the development of chemical admixtures in Japan. *J Adv Concr Technol* 4:211–223. <https://doi.org/10.3151/jact.4.211>
4. Ma Y, Li W, Jin M, Liu J, Zhang J, Huang J, Lu C, Zeng H, Wang J, Zhao H, Tang J (2022) Influences of leaching on the composition, structure and morphology of calcium silicate hydrate (C–S–H) with different Ca/Si ratios. *J Build Eng* 58:105017. <https://doi.org/10.1016/j.job.2022.105017>
5. Kronlif A, Leivo M, Sipari P (1995) Experimental study on the basic phenomena of shrinkage and cracking of fresh mortars. *Cem Concr Res* 25:1747–1754
6. Löfgren I, Jensen OEM, Lura P, Kovler K (2006) Early age cracking of self-compacting concrete. In: International RILEM conference on volume changes of hardening concrete: testing and mitigation, Denmark.
7. Qian X-Q, Zhan S-L, Zhu Y-T (2009) Influence of superplasticizer and shrinkage-reducing admixtures on early age shrinkage of concrete. *Key Eng Mater* 405:166–173
8. Ran Q, Miao C, Liu J, Wu S, Shen J (2006) Performance and mechanism of a multi-functional superplasticizer for concrete. *Mater Trans* 47:1599–1604. <https://doi.org/10.2320/matertrans.47.1599>
9. Ribeiro AB, Goncalves A, Carrajola A (2006) Effect of shrinkage reducing admixtures on the pore structure properties of mortars. *Mater Struct* 39:179–187. <https://doi.org/10.1617/s11527-005-9012-9>
10. Tazawa E, Miyazawa S (1995) Influence of cement and admixture on autogenous shrinkage of cement paste. *Cem Concr Res* 25:281–287. [https://doi.org/10.1016/0008-8846\(95\)00010-0](https://doi.org/10.1016/0008-8846(95)00010-0)
11. Bentz DP, Jensen OM (2004) Mitigation strategies for autogenous shrinkage cracking. *Cem Concr Compos* 26:677–685. [https://doi.org/10.1016/S0958-9465\(03\)00045-3](https://doi.org/10.1016/S0958-9465(03)00045-3)
12. Brian LC, George ER (2001) Reducing drying shrinkage of bridge-deck concrete. *Concr Int* 23:76–82
13. He Z, Li ZJ, Chen MZ, Liang WQ (2006) Properties of shrinkage-reducing admixture-modified pastes and mortar. *Mater Struct* 39:445–453. <https://doi.org/10.1617/s11527-005-9004-9>
14. Bentz DP (2006) Influence of shrinkage-reducing admixtures on early-age properties of cement pastes. *J Adv Concr Technol* 4:423–429. <https://doi.org/10.3151/jact.4.423>
15. Rajabipour F, Sant G, Weiss J (2008) Interactions between shrinkage reducing admixtures (SRA) and cement paste's pore solution. *Cem Concr Res* 38:606–615. <https://doi.org/10.1016/j.cemconres.2007.12.005>
16. Ma H, Zhu H, Wu C, Fan J, Yang S, Hang Z (2021) Effect of shrinkage reducing admixture on drying shrinkage and durability of alkali-activated coal gangue-slag material. *Constr Build Mater*. <https://doi.org/10.1016/j.conbuildmat.2020.121372>
17. Lopes ANM, Silva EF, Dal Molin DCC, Toledo Filho RD (2013) Shrinkage-reducing admixture: effects on durability of high-strength concrete. *ACI Mater J* 110:365–374



18. Mora-Ruacho J, Gettu R, Aguado A (2009) Influence of shrinkage-reducing admixtures on the reduction of plastic shrinkage cracking in concrete. *Cem Concr Res* 39:141–146. <https://doi.org/10.1016/j.cemconres.2008.11.011>
19. Zuo W, Feng P, Zhong P, Tian Q, Gao N, Wang Y et al (2017) Effects of novel polymer-type shrinkage-reducing admixture on early age autogenous deformation of cement pastes. *Cem Concr Res* 100:413–422. <https://doi.org/10.1016/j.cemconres.2017.08.007>
20. Yang G, Wang J, Li H, Yao T, Wang Y, Hu Z et al (2022) Creep behavior of self-compacting rubberized concrete at early age. *J Mater Civ Eng*. [https://doi.org/10.1061/\(asce\)mt.1943-5533.0004091](https://doi.org/10.1061/(asce)mt.1943-5533.0004091)
21. Qianjin Mao JM, Wang Z, Lan M, Cui S (2021) Shrinkage reduction of cement-based materials containing polycarboxylate superplasticiser. *Mag Concr Res* 73:217–227
22. Mao QJ, Ma JF, Wang ZM, Wu WW, Cui SP (2020) The effect of shrinkage-reducing polycarboxylate superplasticizers in cement-based materials. *J Test Eval* 48:2118–2128. <https://doi.org/10.1520/jte20190174>
23. Zuo W, Feng P, Zhong P, Tian Q, Liu J, She W (2019) Effects of a novel polymer-type shrinkage-reducing admixture on early age microstructure evolution and transport properties of cement pastes. *Cem Concr Compos* 95:33–41. <https://doi.org/10.1016/j.cemconcomp.2018.10.011>
24. Shh SP, Krguller ME, Sarigaphuti M (1992) Effects of shrinkage-reducing admixtures on restrained shrinkage cracking of concrete. *ACI Mater J*. <https://doi.org/10.14359/2593>
25. Wang X, Yang W, Ge Y, Feng D (2020) The influence of shrinkage-reducing agent solution properties on shrinkage of cementitious composite using grey correlation analysis. *Constr Build Mater*. <https://doi.org/10.1016/j.conbuildmat.2020.120194>
26. Zhang J, Ma Y, Wang J, Gao N, Hu Z, Liu J et al (2022) A novel shrinkage-reducing polycarboxylate superplasticizer for cement-based materials: synthesis, performance and mechanisms. *Constr Build Mater* 321:126342. <https://doi.org/10.1016/j.conbuildmat.2022.126342>
27. Jiang M, Chen J, Yang D (2005) Dynamic modulus of cement mortar in sulphate erosion measured by ultrasonic checking. *J Chin Ceram Soc* 33:126–132 ((In Chinese))
28. C1698 standard test method for autogenous strain of cement paste and mortar (2014)
29. Wyrzykowski M, Hu Z, Ghourchian S, Scrivener K, Lura P (2017) Corrugated tube protocol for autogenous shrinkage measurements: review and statistical assessment. *Mater Struct*. <https://doi.org/10.1617/s11527-016-0933-2>
30. Jungwirth P, Tobias DJ (2001) Molecular structure of salt solutions: a new view of the interface with implications for heterogeneous atmospheric chemistry. *J Phys Chem B* 105:10468–10472. <https://doi.org/10.1021/jp012750g>
31. Kumarappa DB, Peethamparan S, Ngami M (2018) Autogenous shrinkage of alkali activated slag mortars: Basic mechanisms and mitigation methods. *Cem Concr Res* 109:1–9. <https://doi.org/10.1016/j.cemconres.2018.04.004>
32. Huang H, Ye G (2017) Examining the “time-zero” of autogenous shrinkage in high/ultra-high performance cement pastes. *Cem Concr Res* 97:107–114. <https://doi.org/10.1016/j.cemconres.2017.03.010>
33. Li Z, Nedeljkovic M, Chen B, Ye G (2019) Mitigating the autogenous shrinkage of alkali-activated slag by metakaolin. *Cem Concr Res* 122:30–41. <https://doi.org/10.1016/j.cemconres.2019.04.016>
34. Qu ZY, Yu QL (2018) Synthesizing super-hydrophobic ground granulated blast furnace slag to enhance the transport property of lightweight aggregate concrete. *Constr Build Mater* 191:176–186. <https://doi.org/10.1016/j.conbuildmat.2018.10.018>
35. Wong HS, Barakat R, Alhilali A, Saleh M, Cheeseman CR (2015) Hydrophobic concrete using waste paper sludge ash. *Cem Concr Res* 70:9–20. <https://doi.org/10.1016/j.cemconres.2015.01.005>
36. Sant G, Lothenbach B, Juilland P, Le Saout G, Weiss J, Scrivener K (2011) The origin of early age expansions induced in cementitious materials containing shrinkage reducing admixtures. *Cem Concr Res* 41:218–229. <https://doi.org/10.1016/j.cemconres.2010.12.004>
37. Weiss J, Lura P, Rajabipour F, Sant G (2008) Performance of shrinkage-reducing admixtures at different humidities and at early ages. *ACI Mater J* 105:478–486
38. Diamond S, Ong S (1994) Effects of added alkali hydroxides in mix water on long-term SO₂-concentrations in pore solution. *Cem Concr Compos* 16:219–226. [https://doi.org/10.1016/0958-9465\(94\)90019-1](https://doi.org/10.1016/0958-9465(94)90019-1)
39. Ye H, Radlińska A (2017) Shrinkage mitigation strategies in alkali-activated slag. *Cem Concr Res* 101:131–143. <https://doi.org/10.1016/j.cemconres.2017.08.025>
40. Mackenzie JK (1950) The Elastic Constants of a Solid containing Spherical Holes. In: Proceedings of the physical society. Section B, vol 63, pp 2–11. <https://doi.org/10.1088/0370-1301/63/1/302>
41. Ballekere Kumarappa D, Peethamparan S, Ngami M (2018) Autogenous shrinkage of alkali activated slag mortars: Basic mechanisms and mitigation methods. *Cem Concr Res* 109:1–9. <https://doi.org/10.1016/j.cemconres.2018.04.004>
42. Lura P, Jensen OM, van Breugel K (2003) Autogenous shrinkage in high-performance cement paste: an evaluation of basic mechanisms. *Cem Concr Res* 33:223–232. [https://doi.org/10.1016/S0008-8846\(02\)00890-6](https://doi.org/10.1016/S0008-8846(02)00890-6)
43. Qu ZY, Yu Q, Ji YD, Gauvin F, Voets IK (2020) Mitigating shrinkage of alkali activated slag with biofilm. *Cem Concr Res*. <https://doi.org/10.1016/j.cemconres.2020.106234>
44. Bentur A, Kung JH, Young JF, Milestone NB, Lawrence FV (1980) Influence of microstructure on the creep and drying shrinkage of calcium silicate pastes silicate decalcium.
45. Zhang W, Hama Y, Na SH (2015) Drying shrinkage and microstructure characteristics of mortar incorporating ground granulated blast furnace slag and shrinkage reducing admixture. *Constr Build Mater* 93:267–277. <https://doi.org/10.1016/j.conbuildmat.2015.05.103>
46. Everetto DH (2019) Manual of symbols and terminology for physicochemical quantities and units, appendix II: definitions, terminology and symbols in colloid and surface chemistry. *Pure Appl Chem*. <https://doi.org/10.1351/pac197231040577>
47. Aligizaki KK (2006) Pore structure of cement-based materials: testing, interpretation and requirements. Taylor and Francis, London



48. Feng P, Miao C, Bullard JW (2016) Factors influencing the stability of AFm and AFt in the Ca-Al-S-O-H system at 25 degrees C. *J Am Ceram Soc* 99:1031–1041. <https://doi.org/10.1111/jace.13971>
49. Diamond S (1975) Long-term status of calcium hydroxide saturation of pore solutions in hardened cements. *Cem Concr Res* 5:607–616. [https://doi.org/10.1016/0008-8846\(75\)90061-7](https://doi.org/10.1016/0008-8846(75)90061-7)
50. Mounanga P, Baroghel-Bouny V, Loukili A, Khelidj A (2006) Autogenous deformations of cement pastes: part I. Temperature effects at early age and micro–macro correlations. *Cem Concr Res* 36:110–122. <https://doi.org/10.1016/j.cemconres.2004.10.019>
51. Baroghel-Bouny V, Mounanga P, Khelidj A, Loukili A, Rafai N (2006) Autogenous deformations of cement pastes: part II. W/C effects, micro–macro correlations, and threshold values. *Cem Concr Res* 36:123–136. <https://doi.org/10.1016/j.cemconres.2004.10.020>
52. Coussy O (2006) Deformation and stress from in-pore drying-induced crystallization of salt. *J Mech Phys Solids* 54:1517–1547. <https://doi.org/10.1016/j.jmps.2006.03.002>
53. Sun Z, Scherer GW (2010) Effect of air voids on salt scaling and internal freezing. *Cem Concr Res* 40:260–270. <https://doi.org/10.1016/j.cemconres.2009.09.027>
54. Bentz DP, Garboczi EJ, Quenard DA (1998) Modelling drying shrinkage in reconstructed porous materials: application to porous Vycor glass. *Modell Simul Mater Sci Eng* 6:211–236. <https://doi.org/10.1088/0965-0393/6/3/002>
55. Sant G, Dehadrai M, Lura P, Bentz D, Ferraris CF, Bullard JW et al (2009) Detecting the fluid-to-solid transition in cement pastes: assessment techniques. *Concr Int* 31:53–58
56. Grasley ZC, Scherer GW, Lange DA, Valenza JJ (2007) Dynamic pressurization method for measuring permeability and modulus: II. Cementitious materials. *Mater Struct* 40:711–721. <https://doi.org/10.1617/s11527-006-9184-y>

Publisher's Note Springer Nature remains neutral with regard to jurisdictional claims in published maps and institutional affiliations.

